Vol. 92 No. 1 pp. 367–377 ACTA GEOLOGICA SINICA (English Edition) Feb. 2018

Asian Hydroclimate Changes and Mechanisms in the Preboreal from an Annually-laminated Stalagmite, Daoguan Cave, Southern China

LIU Shushuang, LIU Dianbing*, WANG Yongjin and ZHAO Kan

College of Geography Science, Nanjing Normal University, Nanjing 210023, China

Abstract: One-year-resolved and annually-counted stalagmite multi-proxies ($\delta^{18}O$, $\delta^{13}C$, and layer width) from Daoguan Cave, Guizhou Province revealed detailed variability regarding the Asian Summer Monsoon (ASM) and local humidity across Bond events (BE) in the Preboreal. During BEs 8 and 7, 1.5‰ enrichments in $\delta^{18}O$ values were generally consistent with high- to low-latitude climate changes. In detail, the decadal-scale minor $\delta^{18}O$ oscillations in BE8 were broadly less than the mean value, in contrast to the significant changes in local soil moisture derived from the $\delta^{13}C$ values and layer records. In the mid-BE7, $\delta^{18}O$ variability was generally above the average level, and higher- amplitude variations were observed in the three proxy indicators. Wavelet analysis on the total $\delta^{18}O$ time series and across the specific time windows of BEs 8 and 7 identified periodicities of about 130, 60, and 20-a, respectively. Exceptionally strong in BE7, the 60-a cycle, pervasively observed in instrumental studies, became prominent starting at 11.4 kaBP. Thus, glacial background conditions are important for suppressing the ASM intensity in BE8, while during BE7, tropical hydrological circulations were potentially actively involved. Consequently, climate internal oscillations, analogous to modern conditions, might have occurred in the distant past once the link between the tropical ocean and atmosphere was established as occurs today.

Key words: Daoguan Cave, the Preboreal, Bond Event, ASM, global changes

1 Introduction

In early Holocene, the Preboreal climate stage (11.5–10 kaBP) represented a transitional period between the last glacial period and the Holocene. Climate amelioration during this time was interrupted by two Bond Events (BE). BE7 (10.3 kaBP), and BE8 (11.1 kaBP) have been reported to punctuate the stable Holocene at a pace of ~1500 years (Bond et al., 1997). In Europe, climate instabilities in the Preboreal were intensively investigated during a workshop sponsored by the Royal Netherlands Academy of Arts and Science and the Hugo de Vries foundation (Hoek and Bos, 2007; and the references therein), where it was suggested that two cold and one arid episode existed in the Netherlands (Bohncke and Hoek, 2007). In northern and southern China, percentages of pollen assemblages from the Maar lakes revealed multiple oscillations between 12 and 10 kaBP, indicating that appreciable changes occurred in the regional climates and environments (Stebich et al., 2009; Sheng et al., 2017). However, in the geologic record, such climate variability has different spatial expressions and internal structures that point to divergent dynamic processes (Rasmussen et al., 2007; Wanner et al., 2011). Thus, high-resolution and precisely-dated records are needed to further detect the internal structure of abrupt climate changes that occurred in the Preboreal.

Throughout the Holocene, the imprints of BEs have pervasively been identified in speleothem records (Wang et al., 2005; Fleitmann et al., 2008; Liu et al., 2013). At Heshang Cave, the climate anomaly occurring at 8.2 kaBP appears strikingly intense (about 1.7‰ in the isotopic data) (Liu et al., 2013), but falls within the magnitude of other climate events that occurred in the early Holocene at the Qingtian site (Liu et al., 2015). This indicates that much remains to be reconciled before the physical mechanisms underlying the events can be deduced. Here, we present data on a 237-cm-long stalagmite from Daoguan Cave, southern China. The visible bands are clear in the upper section (from the top to 74.8 cm), which grew between 11.8 and 10.3 kaBP. The general pattern of regional climate and local environment changes occurring

* Corresponding author. E-mail: ldb9921@njnu.edu.cn

since 15 kaBP has been reported elsewhere (Liu et al., 2017). In this study, we further analyzed the internal structure of the BEs in the Preboreal.

2 Site, Samples and Analytical Methods

Daoguan Cave (26º2.7′N, 105º3.4′E, 1420 m a.s.l.) is located in the Yun-Gui Plateau, Guizhou Province, southern China (Fig. 1). The cave is approximately 900 m long, and is overlain by about 30 m of Triassic limestone bedrock. Local precipitation distinctly increases in the late spring as the Indian monsoon intensifies. In summer, regional meteorological conditions are dictated by both the Indian and East Asian Summer Monsoons (ASM). The mean annual temperature at the site is about 14°C, with a maximum in July (20.8°C), and a minimum in January (4.3° C). The annual precipitation is about 1400 mm, peaking (900 mm) during the summer (June through September), and then reaching a minimum (80 mm) in the winter (December to February). Changes of the isotopic composition of precipitation from a nearby meteorological station (Guiyang, 26°35′N, 106°43′E; elevation=1071 m, 190 km NE of Daoguan Cave) reveal a clear seasonal cycle. The mean values of precipitation $\delta^{18}O$ are lower (average ~ −9.93‰, VSMOW) during the summer, than in the winter (average ~ −4.26‰, VSMOW).

Stalagmite DG24 is about 237 cm long, with a stable growth axis (Fig. 2). Visible bands can be observed with the naked eye throughout the upper 74.8 cm, and the layer couplets are composed of white-porous and transparent-compact calcite (Figs. 2b–2d). Detailed descriptions of the site environment and samples can be found in Liu et al. (2017).

For U-Th dating, five sub-samples were collected from the upper 74.8 cm of the stalagmite. The procedures used for the chemical separation and purification of uranium and thorium are similar to those described in Cheng et al. (2000). Measurements were performed using a Multi-Collector Inductively Coupled Plasma Mass Spectrometer (MC-ICP-MS, Thermo-Finnigan Neptune) at the Institute of Global Environmental Change, Xi'an Jiaotong University, China. The dating results are listed in Table 1. The results are within the typical analytical error range (2σ) of less than 260 years. In this study, 485 sub-samples were collected for stable isotopic analysis from two sections spanning 6.4 to 18.6 cm, and 60.8 to 72.8 cm. The spatial resolution was 0.5 mm, equivalent to an average temporal resolution of 1 year. The analyses were performed at the Isotope Laboratory of Nanjing Normal University on a Finnigan MAT-253 mass spectrometer. The precision of the $\delta^{18}O$ values were 0.06‰, and 0.03‰ for $\delta^{13}C$, at the 1-sigma level.

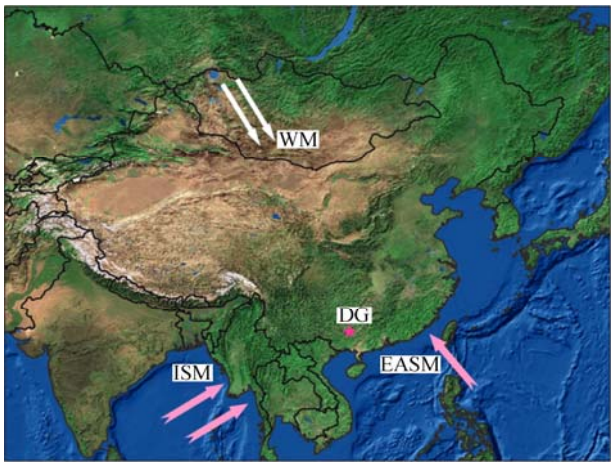

Fig. 1. Location and monsoon situation of Daoguan Cave.
White arrows indicate the direction of winter monsoon (WM), and pink arrows show the Indian summer monsoon (ISM) and eastern Asian summer monsoon (EASM).

Band counting was performed using the Acu-Rite measurement system, which is frequently applied for tree-ring counting. Four duplicate counts along different transects yielded a total of 1460±40 bands in the upper 74.8 cm. In each couplet, the white-porous portion (summertime deposition) was about two to three times more transparent (Figs. 2b–2d). Counting uncertainties may arise due to less distinct layer divisions, as well as from the occurrence of transparent calcite at about 3, 4.5, 9.5, and 35 cm (red triangles in Fig. 2a), which made counting difficult at these depths.

3 Results

The ages for our densely-sampled $\delta^{18}O$ and $\delta^{13}C$ records across BEs7 and 8 were reconstructed from the lamina chronology. In this study, two age models (counted and modeled) were provided for comparison as discussed in Liu et al. (2017). The modeled age was determined using the algorithm MOD-AGE (Hercman and Pawlak, 2012), which uses the locally weighted scatterplot smoothing method (Fig. 3a). A better agreement between the counted and modeled ages can be realized by adjusting the band chronology to the modeled age within the 95% confidence interval as shown in Fig. 3a. In the MOD-AGE software, the Monte Carlo method is used to estimate the confidence bands. For the laminated part of the stalagmite (the upper 74.8 cm), a larger offset between the two age models occurred at about the top (95 years), and 74.8 cm (118 years) (Fig. 3a), which is significantly smaller than the overall dating error of 260 years (Table 1). Thus, a maximum age uncertainty of ±300 years was estimated for the final lamina chronology (including dating errors and counting uncertainties). As the model was strictly dependent on the dating results, the floating lamina

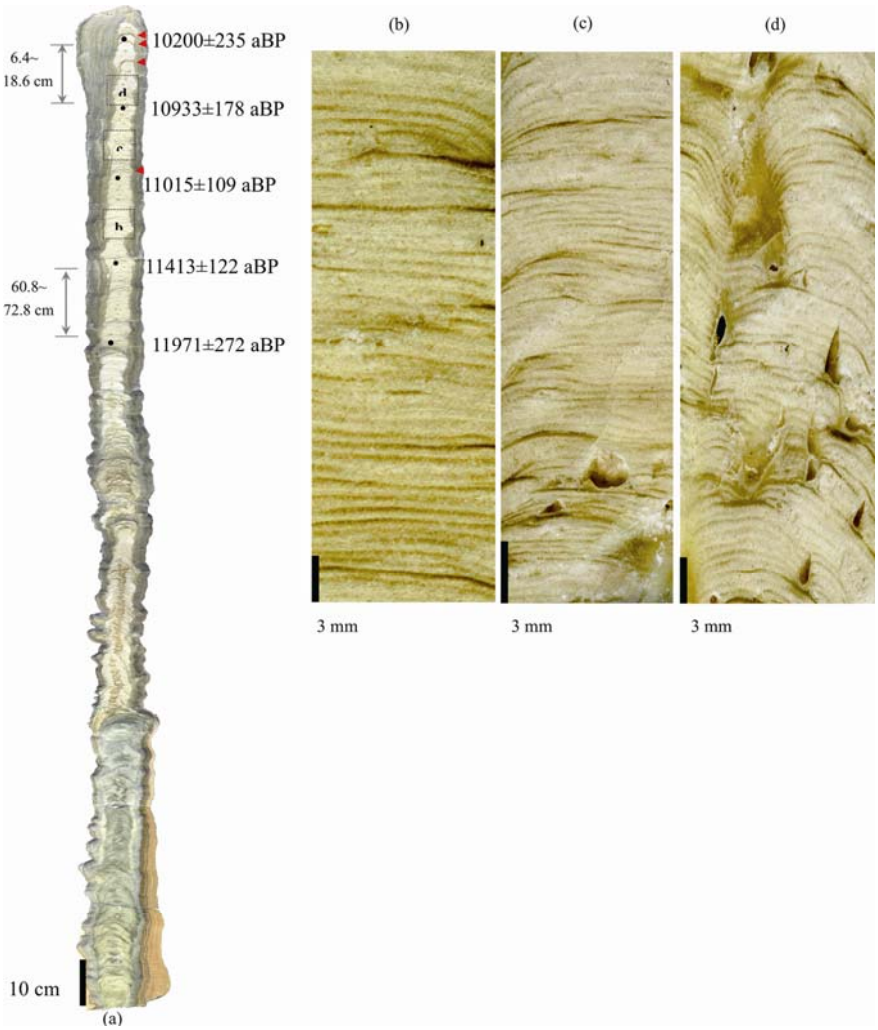

Fig. 2. Photos of Sample DG24 (a) from Daoguan Cave, southern China, and the layer couplets in the upper 74.8 cm (b–d). Dating results are indicated on the stalagmite (black dots), and two sections where densely-sampled analysis undertaken in this study is illustrated on the left. Red triangles indicate the depths where dark-compact calcite occurs and the layer counting is difficult. Dotted rectangles b, c, and d represent the depths at which the enlarged profiles of laminae on the right were chosen.

Table 1 ^{230}Th dating results for Sample DG24 from Daoguan Cave, southern China

Sample number	Depth (cm)	^{238}U (ppb)	^{232}Th (ppt)	δ^{234}U (measured)	^{230}Th/^{238}U (activity)	^{230}Th age (aBP) (uncorrected)	^{230}Th age (aBP) (corrected)	$\delta^{234}U_{Initial}$ (corrected)
DG24-27	2.7	42.8±0.1	243±4	685.0±6.1	0.1527±0.0032	10297±230	10200±235	705.0±6.3
DG24-200	20	44±0	425±9	585.0±1.8	0.1552±0.0017	11172±128	10933±178	603±2
DG24-400	40	45±0	231±5	536.0±1.5	0.1504±0.0011	11175±85	11015±109	553±2
DG24-600	60	46±0	238±5	456.1±1.4	0.1474±0.0012	11579±98	11413±122	471±1
DG24-739	73.9	40.1±0.2	364±4	789.3±11.6	0.1896±0.0037	12117±263	11971±272	816.5±12.1

Errors are 2σ analytical errors. Decay constant values are λ_{230}=9.1577×10^{-6} a^{-1}, λ_{234}=2.8263×10^{-6} a^{-1}, λ_{238}=1.55125×10^{-10} a^{-1}. Corrected ^{230}Th ages assume an initial ^{230}Th/^{232}Th atomic ratio of (4.4±2.2) ×10^{-6}. Corrected ^{230}Th ages are indicated in bold.

chronology we applied can be further adjusted if more high-precision U/Th dates become available.

Isotopic measurements performed on the depths covering the two BEs (6.4 to 18.6 cm and 60.8 to 72.8 cm) showed a striking resemblance to the previous record sampled at 2 mm intervals (Fig. 3b). Changes in the δ^{18}O values were mainly within the range of −10‰ to −8.5‰ during BE8, and −11.5‰ to −9.5‰ during BE7. However, δ^{13}C changes across the two-time windows, not exhibiting a long-term trend as observed for the δ^{18}O signal, consistently fell within an amplitude envelope of −10‰ to −7‰, reflecting different dynamics, or response modes for the two isotopic signals. In detail, the 0.5 mm sampled result revealed distinctly decadal variability with a larger amplitude, and was more enriched than the previous record. This feature was observed both in the δ^{18}O and δ^{13}C records (green curves in Fig. 3b).

As the laminae in Sample DG24 were generally 0.4 to 0.8 mm thick (Fig. 3b), one possibility for why the isotopic values of the new records were more enriched

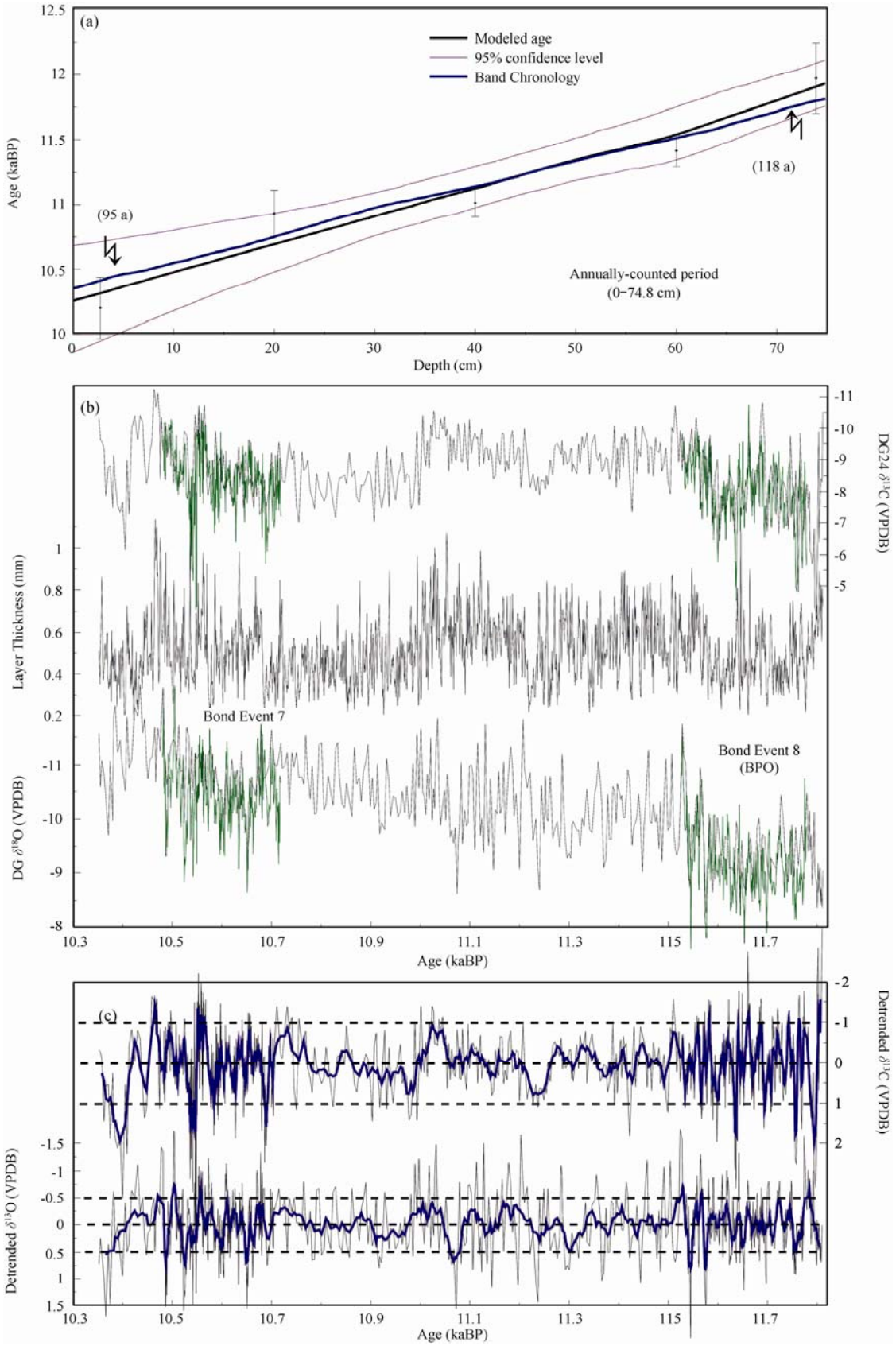

Fig. 3. The age model and isotopic data for the upper 74.8 cm of Sample DG24.

(a), The lamina chronology was applied in this study in comparison with the modeled age as discussed in Liu et al. (2017); (b), Comparison between previous 2-mm-sampled (gray line) and new 0.5-mm-sampled (green line) isotopic data and layer width; (c), detrended stacked isotopic data. The purple curves and gray dashed lines show 9-point running means and the boundaries of these isotopic changes. Note that BES 8 and 7 are not strikingly clear in the detrended data, which are characterized by decadal oscillations.

might be related to wintertime deposition, which is the result of winter rainfall with relatively positive isotopic values. Dynamically, speleothem $\delta^{18}O$ values can trace the isotopic composition of local rainfall, and the $\delta^{13}C$ signal can reflect the soil CO_2 production associated with plant respiration and microbiological decomposition (Genty et al., 2003). In winter, the positive precipitation $\delta^{18}O$ values and weaker biological activity (resulting in enriched soil $^{13}CO_2$) can partly explain the deviation between our previous studies and the new records. This interpretation may hold true for some calcite subsamples, but not all, as the transparent portion (grown in winter) contributed insignificantly to the layer couplets (Figs. 2b–2d). Thus, we believe that seasonal bias is not a satisfactory explanation, and the new record is mainly a proxy for the detailed climatic and environmental changes which dominate the cave site, although, site-specific noise is probably included in the data.

In our new record, $\delta^{18}O$ enrichments during BEs8 and 7 are within an amplitude of about 1.5‰ (Fig. 3b). However, multi-decadal to decadal oscillations are large in magnitude (about 1‰ to 1.5‰), making the two BEs less prominent. When the original and 0.5 mm sampled isotopic data are pieced together and detrended, the remaining $\delta^{13}C$ values change at about a magnitude of 2‰, while the $\delta^{18}O$ variability is only about 1‰ (Fig. 3c). As such, the two BEs are not strikingly significant in the detrended $\delta^{18}O$ series. If the ±0.5‰ is taken as an envelope, $\delta^{18}O$ value changes during these periods fall well within the range of the full sequence. Thus, the observation of the $\delta^{18}O$ variability during BEs 8 and 7 (absence of abnormality in comparison with the original series in Fig. 3b) is likely attributed to pronounced decadal -scale fluctuations, which characterize both our previous and new records.

4 Discussion

4.1 Regional correlation of BEs7 and 8

The BEs, first identified in North Atlantic sediment records, refer to climate instabilities in the Holocene with a periodicity of 1500 years, and were believed to have the same common dynamic origin as millennial-scale climate changes that occurred during the last glacial period (Bond et al., 1997). However, these Holocene climate instabilities are weaker in magnitude and shorter in duration than those from the last glacial period. Hence, more precise age controls and high-resolution data are needed to constrain the durations and internal structures. For example, the climate anomaly around 8.2 kaBP (also termed as BE5) is frequently expressed as a long-term cooling that spanned 400 to 600 years at the mid- to low-latitudes, which is inconsistent with the severe Greenland temperature decline (Rohling and Pälike, 2005).

Between 11.8±0.3 kaBP and 10.3±0.3 kaBP, the annually-counted DG24 $\delta^{18}O$ record shows a long-term depletion trend, concomitant with northern warming/ wetting and a rise in the relative sea-level (Liu et al., 2017). This indicates that speleothem $\delta^{18}O$ values are a proxy of regional climate, likely associated with the background circulation of regional climates, i.e., the averaged intensity of the ASM (Tan, 2016; Yan and Tan, 2016). An actively-grown stalagmite from Huanglong Cave, eastern Qinghai-Tibet Plateau showed that calcite $\delta^{18}O$ values can closely trace monsoon-laden meteoric precipitation isotopic compositions (Yang et al., 2007). Superimposed on this trend, the range of two $\delta^{18}O$ enrichment events at about 11.7 and 10.6 kaBP reached 1.5‰ to 2‰ in our densely-sampled data (Fig. 4a), corresponding to BEs8 and 7. Within the dating uncertainties, these ASM depressions agree well with the decline in the Indian summer monsoon derived from sediment reflectance from the Arabian Sea (Fig. 4b) (Deplazes et al., 2013), the increase in Ca^{2+}-based Asian winter monsoon (Fig. 4c) (Mayewski et al., 1997), and the decrease of high-latitude surface temperatures from Greenland ice-cores (Fig. 4d) (Rasmussen et al., 2006). These observations illustrate that climate instabilities across BEs are not a local phenomenon restricted to the North Atlantic region, but have a far-field effect, at least extending to the hemispheric scale.

However, regional expressions of BEs are possibly variable. Among these records, BEs8 and 7 are clearly observed in the DG24 stalagmite and the North Greenland Ice-core Project (NGRIP) $\delta^{18}O$ records (Rasmussen et al., 2006) (Figs. 4a, 4d). In the Arabian sediment record, both events are weaker in amplitude (Deplazes et al., 2013) (Fig. 4b). The Greenland Ice Sheet Project 2 (GISP2) Ca^{2+} concentration data increased significantly around BE8, but only slightly at BE7 (Mayewski et al., 1997) (Fig. 4c). Moreover, another Greenland temperature drop at 10.95 kaBP (termed as BE8.1 in this study), although lesser in degree than the two major BEs, is not captured by the Ca^{2+} record, but is equally well reflected in the Arabian and our speleothem records. Regardless of the inconsistency in sources and the climatic interpretations for these proxy indicators, the relationship observed in Figure 4, at least, suggests that regional climate responses during the Holocene were more complicated than in the last glacial period.

4.2 Internal structure of BEs7 and 8

Following the procedures proposed by Thomas et al. (2007), the mean values and standard deviations of the 500

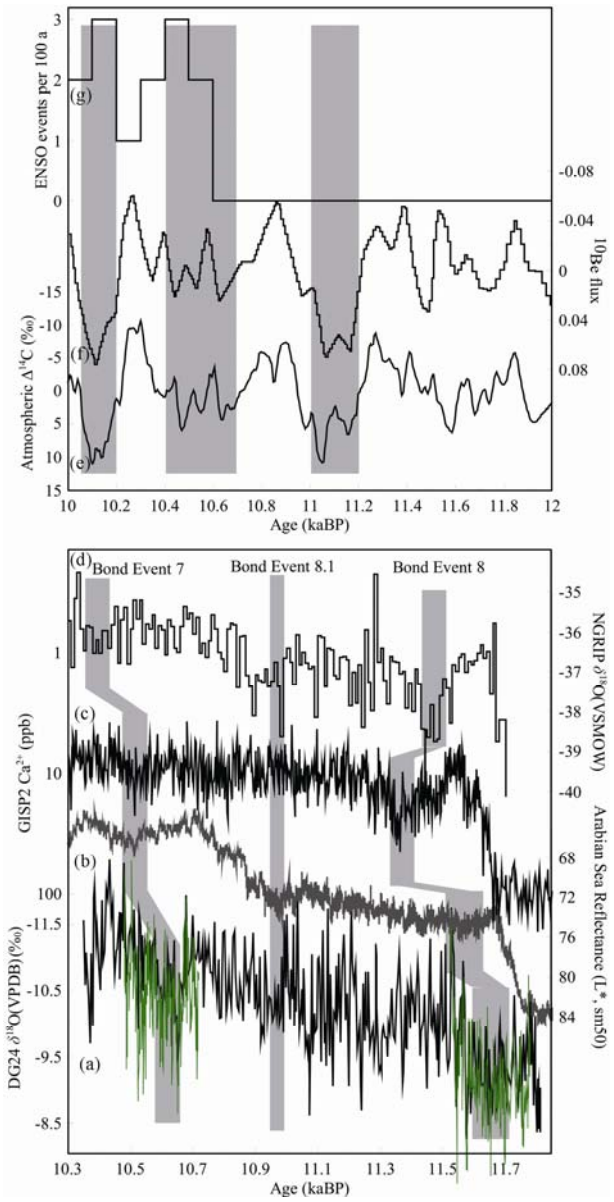

Fig. 4. Regional correlation of BEs 8 and 7, and the dynamic link between ASM and solar activity, tropical processes.

(a), DG24 δ^{18}O record; (b) Sediment reflectance from Arabian Sea (Deplazes et al., 2013); (c), GISP2 Ca^{2+} record (Mayewski et al., 1997); (d), NGRIP ice δ^{18}O record (Rasmussen et al., 2006). The gray bars illustrate the possible link between them across BEs 8 and 7, and surrounding 10.95 kaBP; (e), Atmospheric ^{14}C concentration (Reimer et al., 2013); (f), ^{10}Be flux from Greenland ice cores (Muscheler et al., 2004); (g), the ENSO frequency (Moy et al., 2002). Three gray bars in Figs 3e–3f show periods of decreased solar activity.

-year stacked isotopic data surrounding BEs8 and 7 were calculated and used as reference values (Figs. 5a, 5b), therefore allowing the onset and end points for BE8 to be estimated as 11.77±0.3 and 11.57±0.3 kaBP, and 10.67±0.3 and 10.52±0.3 kaBP for BE7. At the onset of BE8, the δ^{18}O values increase from −10.7‰ to −8.1‰ within 17 years, and at the end, decrease from −7.8‰ to −10.7‰ within 10 years. Early during BE7, δ^{18}O values shift from −11.5‰ to −9.3‰ over 10 years, and decrease from −8.8‰ to −11.2‰ in only 2 years at the termination of the event. Generally, most isotopic data shifts were between −8.5‰ and −10‰ during BE8, and −9.5‰ to −11‰ for BE7, each within a similar range of 1.5‰. In the early Holocene, climate changes of similar magnitude have been widely reported, i.e., by two coeval stalagmites from Austria (Boch et al., 2009) and four annually-laminated stalagmites from Qingtian Cave, in central China (Liu et al., 2015). Among BEs8 and 7, decadal δ^{18}O oscillations with an amplitude of over 1‰ were strikingly clear. Nevertheless, detailed patterns for these minor sub-cycles are differently registered in the two events. First, decadal ASM variability during BE8 is mostly below the mean value, but above the average level in BE7. Second, a 'W' structure can be observed in the BE7 δ^{18}O profile. At mid-BE7, a measurable ASM decline (lasting two decades with a magnitude of 1.5‰) was prominent at about 10.6 kaBP, separated by two periods of multi-decadal ASM strengthening. In contrast, the δ^{18}O fluctuations in BE8 were relatively stable, broadly constrained by an envelope of −9.5‰ to −8.5‰. This suggests that the BE7 ASM shows much higher variability, while in BE8 the ASM was probably constrained by glacial background conditions (Dharmendra Pratap Singh et al., 2017; Qi Lin et al., 2017).

Changes of speleothem δ^{13}C values and layer thickness records were believed to be a site-specific phenomenon (Fairchild et al., 2006; Tan et al., 2006; Baker et al., 2008) or climatically dependent (Hu et al., 2001; Genty et al., 2003; Tan et al., 2003), because the soil moisture, local temperature, degassing rate in the cave, the soil CO_2 production determined by vegetation type, density and microbiological activities, are all a prerequisite for δ^{13}C and layer thickness variations. In Figures 5c and 5d, the coeval δ^{13}C values and band records show considerable inconsistency compared with the δ^{18}O variability. During BE8, the more negative δ^{13}C values with higher variability at about 11.68 kaBP are synchronous with a period of thicker layers, and enriched δ^{13}C values at 11.6 kaBP correspond to thinner bands (crossed bars in Fig. 5d). During these periods, the δ^{18}O record was characterized by smaller oscillations around −9‰. Nevertheless, at the onset of BE8, a decline in the ASM is more or less reflected in the δ^{13}C values and band records, although the duration of the ASM depression was relatively longer (blue bar in Fig. 5d). Surrounding BE7, two weak ASM events (at about 10.69 and 10.53 kaBP) are well mirrored in the δ^{13}C values and band records (blue bars in Fig. 5c). However, δ^{18}O enrichments (weak ASM) at 10.65 kaBP did not match the depleted δ^{13}C values (higher soil CO_2 production) and thicker layers (crossed bar in Fig. 5c).

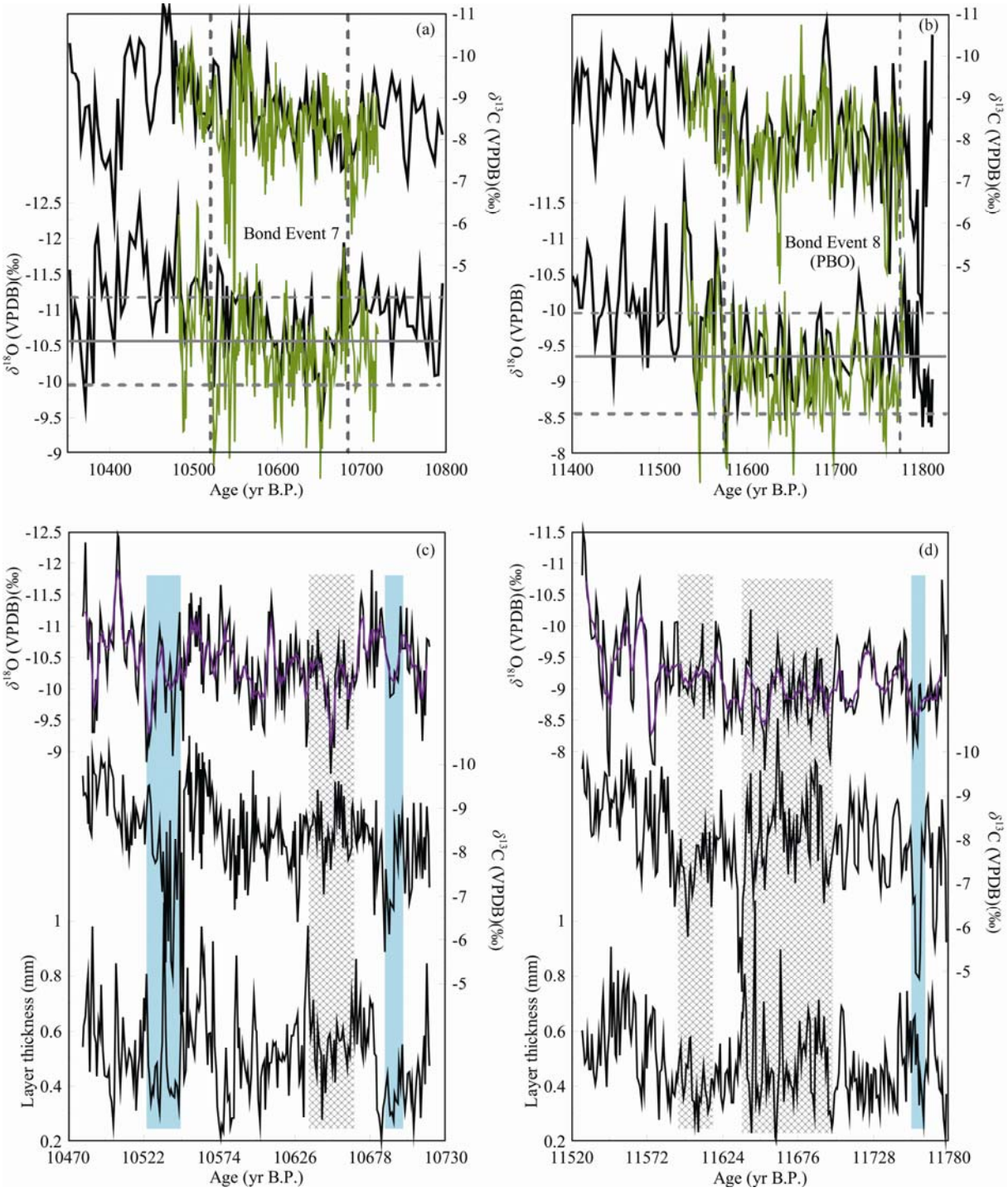

Fig. 5. Detailed comparison between δ^{18}O, δ^{13}C and layer records across BEs 8 and 7.
In Panels a and b the onsetting and ending timings for two events were determined using a method by Thomas et al. (Thomas et al., 2007). The solid gray and horizontal dashed lines represent the mean values and standard deviations of 500-year stacked isotopic data around these events. The vertical dashed lines label the onset and end. Panels c and d show a detailed comparison between δ^{18}O, δ^{13}C and layer records across these events. The blue bars illustrate synchronous changes between them, and the crossed bars show inconsistency.

Among the three proxy indicators, δ^{13}C value changes showed considerable similarity to the band record, implying that they should share a common forcing mechanism in contrast to the δ^{18}O signal.

These detailed comparisons between δ^{18}O, δ^{13}C, and layer records imply that the speleothem δ^{18}O values represent a proxy of regional significance (i.e., the ASM) as observed in Figure 4, while the latter two may be related to site-specific processes. Disagreement between the calcite δ^{18}O and δ^{13}C records has recently been observed at the Wulu Cave, southern China (Liu et al., 2013; Liu et al., 2016) and the Hulu Cave, eastern China

(Kong et al., 2005), in which millennial-scale $\delta^{18}O$ variability is clear in the last glacial period, but the $\delta^{13}C$ signal is characterized by persistently centennial-scale oscillations. Rocky desertification and soil erosion are severe in the southwestern Guizhou Province (AU and Yang, 2013; Jiang et al., 2014). The soil cover at the Daoguan site is thin and patchily-distributed, and the modern vegetation is mostly composed of shrubs and deciduous herbs, hence, the local rainfall or precipitation/ evaporation (P/E) ratio is likely a prominent limiting factor for changes in the $\delta^{13}C$ values and layer width (Liu et al., 2017). This idea is supported by speleothem records from Central Asia that indicate carbon isotope and trace element data can reflect local hydroclimatic variability (Cheng et al., 2016). Therefore, one-year-resolved and annually-counted DG24 records revealed that although glacial backgrounds were important for suppressing the ASM variability during BE8, the level of P/E or soil moisture might be high, resulting in higher soil CO_2 production and larger annual deposition in the mid-BE8 (Fig. 5d). During the BE7, higher variability in the three proxy indicators (Fig. 5c), however, suggests that the constraining effect of averaged climate state on the ASM was alleviated. In Bolivia, the tropical glaciers retreated rapidly from 10.8±0.9 kaBP (Jomelli et al., 2011), suggesting a significant warming at this time and an addition of tropical ocean-atmosphere interactions. These factors could enhance the ASM intensity and soil CO_2 production during BE7, as evidenced by Figure 5c.

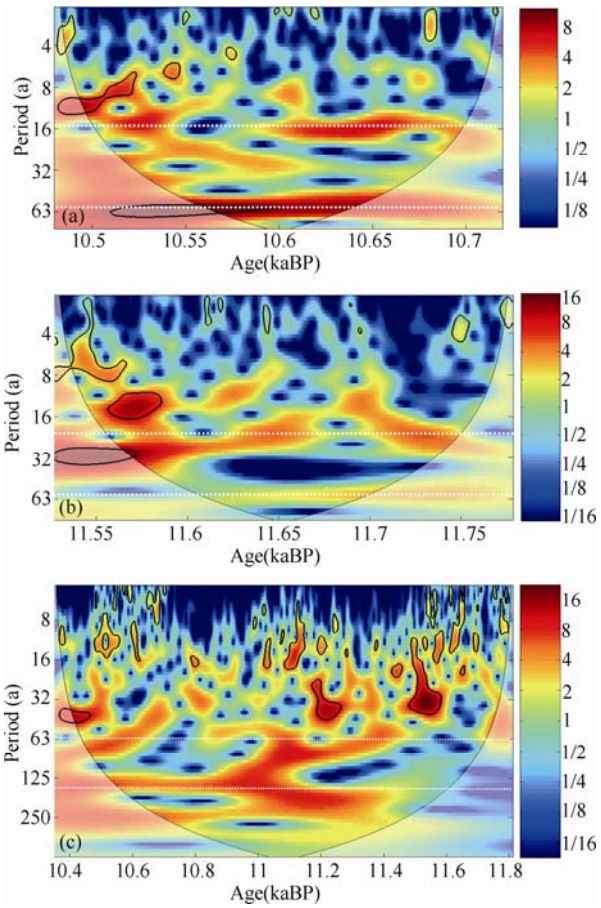

Fig. 6. Wavelet analysis on the detrended $\delta^{18}O$ time series in the Preboreal (c), during BE7 (a) and BE8 (b).
In the total sequence, two cycles of about 130 and 60 years are evident since 11.4 kaBP. During BEs 8 and 7, periodicities of 20 and 60 years were detected. In these analyses, the 60-year cycle is strikingly prominent in BE7.

4.3 External and internal forcing of ASM in the Preboreal

Spectral analysis on the detrended full $\delta^{18}O$ series revealed that two cycles are evident in the Preboreal, i.e., 130 and 60 years (Fig. 6c). The 60-year cycle first occurred at about 11.4±0.3 kaBP. In our one-year resolved record (including BEs8 and 7), two multi-decadal periodicities were detected, centering at about 60 and 20 years (Figs. 6a and 6b). During BE8 (Fig. 6b), the 60-year spectrum is exceptionally weaker in intensity than in BE7 (Fig. 6a). This 60-year periodicity, pervasive in our previous and new records, is in agreement with the 50–70-year cycles observed in instrumental monsoon precipitation and northern temperature records (Kumar et al., 1999; Delworth and Mann, 2000), which was explained as the result of internal climate oscillations. Furthermore, our ASM reconstruction implies that the internal feedbacks of low-latitude climates were relatively weaker in early Preboreal, and became stronger from 11.4±0.3 kaBP. These observations show that multi-decadal variability is an intrinsic feature for climate changes when ocean-atmosphere interactions are reactivated.

In a broad sense, the Preboreal climate variability should be impacted by climate reorganizations associated with the last deglaciation. During this time window, the ASM intensity had just resumed from the exceptional climate deterioration termed as the Younger Dryas event between 12.9 and 11.5 kaBP (Li et al., 1998; Qin et al., 2005; Yang et al., 2010). Subsequently, the long-term ASM strengthening followed the external forcing (i.e., northern summer insolation) in the Preboreal (Shao et al., 2006; Liu and Shi, 2009). Additionally, in the northern hemisphere, different climate sub-systems exhibited a concurrent response as observed in Figure 4a–4d, indicating an impact from the external forcing. When entering the Holocene, the rapid retreat of continental ice sheets meant that high levels of melting water poured into the oceans (Carlson et al., 2008). It was suggested that freshwater outbursts into the North Atlantic were a major driver for BEs (Bond et al., 1997), and between 12 and 10 kaBP seven freshwater pulses occurred in the North

Atlantic (Teller and Leverington, 2004). If the solar output could affect the production of North Atlantic Deep Water and thus transmit climate signals globally (Bond et al., 2001), there should exist a causal link between solar activity and the ASM. Between 12 and 10 kaBP, three periods of decreased solar activity were identified surrounding 11.1, 10.6, and 10.1 kaBP derived from atmospheric $\Delta^{14}C$ values (Reimer et al., 2013) (Fig. 4e) and Greenland ice-core ^{10}Be flux records (Muscheler et al., 2004) (Fig. 4f). Within the dating uncertainties, only event at 10.6 kaBP matches BE7 in the speleothem record, apparently conflicting with our observation of the comparable ASM decline during BEs8 and 7. Dynamically, solar activity itself is too weak to directly drive climate changes, hence a series of internal feedbacks are needed as an amplifying mechanism, i.e., atmosphere-ocean interactions. The El Niño–Southern Oscillation (ENSO) frequency was very low between 12 and 10.6 kaBP (Moy et al., 2002) (Fig. 4g), subsequently it began to increase until reaching a significant level at 7 kaBP. This implies that although the combined effect of the Atlantic meridional overturning circulation and solar output were responsible for the ASM depressions during BEs8 and 7 (Bond et al., 2001; Teller and Leverington, 2004), higher variability in $\delta^{18}O$ and $\delta^{13}C$ values along with layer width especially in BE7, at least, points to an increased involvement of low-latitude hydrological circulations. This assertion is further supported by the wavelet analysis (Fig. 6). The stronger 60-year cycle in BE7 provides evidence for internal climate oscillations similar to modern conditions. Consequently, the averaged Earth's climate state is important for abrupt climate changes, including the evolution pattern and internal structure.

5 Conclusions

An annually-laminated stalagmite from Daoguan Cave, Guizhou Province provided a multi-proxy study on the internal structure of BEs 8 and 7 in the Preboreal.

(1) Between 11.8±0.3 and 10.3±0.3 kaBP, the general evolution of the ASM intensity and the two ASM depressions surrounding BEs 8 and 7 agrees with other climate records within the northern hemisphere. During these events, the $\delta^{18}O$ records are characterized by decadal oscillations. Most of these sub-cycles during BE 8 are below the mean value, but above the average level in BE 7.

(2) The absolute values of $\delta^{13}C$ records during the two events are both confined to −9‰ to −7‰, which exhibited a similar pattern as changes of the layer thickness. In mid-BE 8, the higher variability of the $\delta^{13}C$ values and the layer thickness are not in agreement with the relatively stable $\delta^{18}O$ record. During BE 7, larger-amplitude changes are evident in the three indicators.

(3) These observations indicate that the local soil moisture balance was not decisively dependent on the ASM intensity. In the latter part of the Preboreal, such as during BE 7, the tropical ocean-atmosphere interactions are more important for changes of the $\delta^{18}O$, $\delta^{13}C$ and layer records.

(4) The wavelet analysis revealed a stronger 60-year cycle from about 11.4±0.3 kaBP. This periodicity is pervasive in modern climate observations and simulations. Thus, the tropical hydrological circulations probably overrode the effect of continental ice-sheets from about 11.4±0.3 kaBP. Another possibility might be related to local climate processes, such as the location of the subtropical high-pressure cell, cyclone activities, and other factors. These contributions are beyond the scope of our study and require further investigations.

Acknowledgements

We are grateful to two anonymous reviewers for their generous technical comments on an early version of this manuscript. This work was jointly supported by grants of National Key R&D Program of China (No. 2016YFA0600401), National Nature Science Foundation of China (No. 41672161), A Project Funded by the Priority Academic Program Development of Jiangsu Higher Education Institutions (PAPD) (164320H116), Jiangsu Center for Collaborative Innovation in Geographical Information Resource Development and Application, and Key Laboratory of Virtual Geographic Environment (Nanjing Normal University).

Manuscript received June 19, 2017
accepted Oct. 17, 2017
edited by Liu Lian

References

Au Yik Yu and Yang Hui, 2013. Analysis of Rocky Desertification and Soil Erosion in Relationship with Rock Type in Guizhou and Guangxi Province. *Acta Geologica Sinica* (English Edition), 87(s1): 932.

Baker, A., Smith, C.L., Jex, C., Fairchild, I.J., Genty, D., and Fuller, L., 2008. Annually laminated speleothems: a review. *International Journal of Speleology*, 37(3): 193–206.

Boch, R., Spötl, C., and Kramers, J., 2009. High-resolution isotope records of early Holocene rapid climate change from two coeval stalagmites of Katerloch Cave, Austria. *Quaternary Science Reviews*, 28(23-24): 2527–2538.

Bohncke, S.J.P., and Hoek, W.Z., 2007. Multiple oscillations during the Preboreal as recorded in a calcareous gyttja, Kingbeekdal, The Netherlands. *Quaternary Science Reviews*, 26(15–16): 1965–1974.

Bond, G., Showers, W., Cheseby, M., Lotti, R., Almasi, P., deMenocal, P., Priore, P., Cullen, H., Hajdas, I., and Bonani, G., 1997. A pervasive millennial-scale cycle in North Atlantic Holocene and glacial climates. *Science*, 278(5341): 1257–1266.

Bond, G., Kromer, B., Beer, J., Muscheler, R., Evans, M.N., Showers, W., Hoffmann, S., Lotti-Bond, R., Hajdas, I., and Bonani, G., 2001. Persistent solar influence on North Atlantic climate during the Holocene. *Science*, 294(5549): 2130–2136.

Carlson, A.E., LeGrande, A.N., Oppo, D.W., Came. R.E., Schmidt, G.A., Anslow, F.S., Licciardi, J.M., and Obbink, E.A., 2008. Rapid early Holocene deglaciation of Laurentide ice sheet. *Nature Geoscience*, 1(9): 620–624.

Cheng, H., Edwards, R.L., Hoff, J., Gallup, C.D., Richards, D.A., and Asmerom.Y., 2000. The half-lives of uranium-234 and thorium-230. *Chemical Geology*, 169(1): 17–33.

Cheng, H., Spötl, C., Breitenbach, S.F.M., Sinha, A., Wassenburg, J.A., Jochum, K.P., Scholz, D., Li X.L., Yi, L., Peng, Y.B., Lv, Y.B., Zhang P.Z., Votintseva, A., Loginov, V., Ning Y.F., Kathayat, G., and Edwards, R.L., 2016. Climate variations of Central Asia on orbital to millennial timescales. *Scientific Reports*, 6: 36975, doi:10.1038/ srep36975.

Delworth, T.L., and Mann, M.E., 2000. Observed and simulated mutidecadal variability in the North Hemisphere. *Climate Dynamics*, 16(19): 661–667.

Deplazes, G., Lückge, A., Peterson, L.C., Timmermann, A., Hamann, Y., Hughen, K.A., Röhl, U., Laj, C., Cane, M.A., Sigman, D.M., and Haug, G.H., 2013. Links between tropical rainfall and North Atlantic climate during the last glacial period. *Nature Geoscience*, 6(3): 213–217.

Dharmendra Pratap Singh, Rajeev Saraswat and Dinesh K.Naik, 2017. Does Glacial-Interglacial Transition Affect Sediment Accumulation in Monsoon-Dominated Regions? *Acta Geologica Sinica* (English Edition), 91(3): 1079–1094.

Fairchild, I.J., Smith, C.L., Baker, A., Fuller, L., Spötl, C., Mattey, D., McDermott, F., and E.I.M.F., 2006. Modification and preservation of environmental signals in speleothems. *Earth-Science Reviews*, 75(1–4): 105–153.

Fleitmann, D., Mudelsee, M., Burns, S.J., Bradley, R.S., Kramers, J., and Matter, A., 2008. Evidence for a widespread climatic anomaly at around 9.2ka before present. *Paleoceanography*, 23: PA1102, doi:10.1029/ 2007PA001519.

Genty, D., Blamart, D., Ouahdi, R., Gilmour, M., Baker, A., Jouzel, J., and Van-Exter., S., 2003. Precise dating of Dansgaard-Oeschger climate oscillations in western Europe from stalagmite data. *Nature*, 421(6925): 833–837.

Hercman, H., and Pawlak, J., 2012. MOD-AGE: An age-depth model construction algorithm. *Quaternary Geochronology*, 12 (12): 1–10.

Hoek, W.Z., and Bos, J.A.A., 2007. Early Holocene climate oscillations–causes and consequences. *Quaternary Science Reviews*, 26(15): 1901–1906.

Hu Chaoyong, Huang Junhua, Yang Guanqing, Lin Xiulun and Fang Nianqiao, 2001. Climate history of the middle reach of the Yangtze river over the past 9000 years: A speleothem isotopic record from Za cave, Hubei, China. *Science in China Series E*, 44(s1): 119–122.

Jiang, Z.C., Lian, Y.Q., and Qin, X.Q., 2014. Rocky desertification in Southwest China: Impacts, cause, and restoration. *Earth-Science Reviews*, 132(3): 1–12.

Jomelli, V., Khodri, M., Favier, V., Brunstein, D., Ledru, M.P., Wagnon, P., Blard, P.H., Sicart, J.E., Braucher, R., Grancher, D., Bourlès, D.L., Braconnot, P., and Vuille, M., 2011. Irregular tropical glacier retreat over the Holocene epoch driven by progressive warming. *Nature*, 474(7350): 196–199.

Kong Xinggong, Wang Yongjin, Wu Jiangying, Cheng Hai, Edwards, R.L., and Wang Xianfeng, 2005. Complicated responses of stalagmite δ^{13}C to climate change during the last glaciation from Hulu Cave, Nanjing, China. *Science in China* (Ser. D Earth Sciences), 48(12): 2174–2181.

Kumar, K.K., Rajagopalan, B., and Cane, M.A., 1999. On the weakening relationship between the Indian and monsoon and ENSO. *Science*, 284(5423): 2156–2159.

Li Bin, Yuan Daoxian, Lauritzen, Stein-Erik., Qin Jiaming and Lin Yushi, 1998. The Younger Dryas Event and Holocene Climate Fluctuations Recorded in a Stalagmite from the Panlong Cave of Guilin. *Acta Geologica Sinica* (English Edition), 72(4): 455–465.

Liu Dianbing, Wang Yongjin, Cheng Hai and Edwards, R.L, 2013. High-resolution stalagmite δ^{13}C record of soil processes from southwestern China during the early MIS 3. *Chinese Science Bulletin*, 58(7): 796–802.

Liu, D.B., Wang, Y.J., Cheng, H, Edwards, R.L., and Kong, X.G., 2015. Cyclic changes of Asian monsoon intensity during the early mid-Holocene from annually-laminated stalagmites, central China. *Quaternary Science Reviews*, 121: 1–10.

Liu, D.B., Wang, Y.J., Cheng, H., Edwards, R.L., and Kong, X.G., 2017. Remote vs. local control on the Preboreal Asian hydroclimate and soil processes recorded by an annually-laminated stalagmite from Daoguan Cave, southern China. *Quaternary International*, 452: 79–90.

Liu Shuhua, Huang Jiayi, Chen Lin, Yang Liang, Chen Qiong, Mi Xiaojian, He Haibo, Deng Xiaomin, Peng Xiaotao, Li Hanjie and Zhou Houyun, 2016. A Speleothem δ^{13}C record and control mechanism during 120~103 kaB.P. from NE Sichuan, Central China. *Acta Geologica Sinica*, 90(2): 334–340 (in Chinese with English abstract).

Liu Xiaodong and Shi Zhengguo, 2009. Effect of precession on the Asian summer monsoon evolution: A systematic review. *Chinese Science Bulletin*, 54(20): 3720–3730.

Liu, Y.H., Henderson, G.M., Hu, C.Y., Mason, A.J., Charnley, N., Johnson, K.R., and Xie, S.C., 2013. Links between the East Asian monsoon and North Atlantic climate during the 8,200 year event. *Nature Geoscience*, 6(2): 117–120.

Mayewski, P.A., Meeker, L.D., Twickler, M.S., Whitlow, S., Yang, Q.Z., Lyons, W.B., and Prentice, M., 1997. Major features and forcing of high-latitude northern hemispheric circulation using a 110000-year-long glaciochemical series. *Journal of Geophysical Research*, 102: 26(C12), 345–26, 366.

Moy, C.M., Seltzer1, G.O., Rodbell, D.T., and Anderson, D.M., 2002. Variability of El Niño/Southern Oscillation activity at millennial timescales during the Holocene epoch. *Nature*, 420 (6912): 162–165.

Muscheler, R., Beer, J., Wagner, G., Laj, C., Kissel, C., Raisbeck, G.M., Yiou, F., and Kubik, P.W., 2004. Changes in the carbon cycle during the last deglaciation as indicated by the comparison of ^{10}Be and ^{14}C records. *Earth and Planetary Science Letters*, 219(3–4): 325–340.

Qi Lin, Qiao Yansong, Li Yuehui, Wang Yan, Peng Shasha, He Zexin, Yang Shuaibin, Han Chao and Zhang Xujiao, 2017. Intensification of the East Asian Monsoon in Southern China

at about 300-400 kaBP Inferred from Eolian Deposits in the Middle-lower Reaches of the Yangtze River. *Acta Geologica Sinica* (English Edition), 91(3):1095–1108.

Qin Jiaming, Yuan Daoxian, Cheng Hai, Lin Yushi, Zhang Meiliang, Wang Fuxing, Edwards, R.L, Wang Hua and Ran Jingcheng, 2005. The Y. D. and climate abrupt events in the early and middle Holocene: Stalagmite oxygen isotope record from Maolan, Guizhou, China. *Science in China* (Ser. D Earth Sciences), 48(4): 530–537.

Rasmussen, S.O., Andersen, K.K., Svensson, A.M., Steffensen, J.P., Vinther, B.M., Clausen, H.B., Siggaard-Andersen, M.L., Johnsen, S.J., Larsen, L.B., Dahl-Jensen, D., Bigler, M., Röthlisberger, R., Fischer, H., Goto-Azuma, K., Hansson, M.E., and Ruth, U., 2006. A new Greenland ice core chronology for the last glacial termination. *Journal of Geophysical Research*, 111: D06102, doi:10.1029/2005JD006079.

Rasmussen, S.O., Vinther, B.M., Clausen, H.B., and Andersen, K.K., 2007. Early Holocene climate oscillations recorded in three Greenland ice cores. *Quaternary Science Reviews*, 26 (15): 1907–1914.

Reimer, P.J., Bard, E., Bayliss, A ., Beck, J.W., Blackwell, P.G., Ramsey, C.B., Buck, C.E., Cheng, H., Edwards, R.L., Friedrich, M., Grootes, P.M., Guilderson, T.P., Haflidason, H., Hajdas, I., Hatte, C., Heaton, T.J., Hoffmann, D.L., Hogg, A.G., Hughen, K.A., Kaiser, K.F., Kromer, B., Manning, S.W., Niu, M., Reimer, R.W., Richards, D.A., Scott, E.M., Southon, J.R., Staff, R.A., Turney, C.S.M ., and van der Plicht, J., 2013. IntCal13 and Marine13 radiocarbon age calibration curves 0-50,000 years cal BP. *Radiocarbon*, 55(4): 1869–1887.

Rohling, E.J., and Pälike, H., 2005. Centenial-scale climate cooling with a sudden cold event around 8,200 years ago. *Nature*, 434(7036): 975–979.

Shao Xiaohua, Wang Yongjin, Cheng Hai, Kong Xinggong, Wu Jiangying and Edwards, R.L, 2006. Long-term trend and abrupt events of the Holocene Asian monsoon inferred from a stalagmite δ^{18}O record from Shennongjia in Central China. *Chinese Science Bulletin*, 51(2): 221–228.

Sheng, M., Wang, X.S., Zhang, S.Q., Chu, G.Q., Su, Y.L., and Yang, Z.Y., 2017. A 20,000-year high-resolution pollen record from Huguangyan Maar Lake in tropical-subtropical South China. *Palaeogeography Palaeoclimatology Palaeoecology*, 472: 83–92.

Stebich, M., Mingram, J., Han, J.T., and Liu J.Q., 2009. Late Pleistocene spread of (cool-) temperate forests in Northeast China and climate changes synchronous with the North Atlantic region. *Global and Planetary Change*, 65(1–2): 56–70.

Tan, M, Liu, T.S., Hou, J.Z., Qin, X.G., Zhang, H.C., and Li, T.Y., 2003. Cyclic rapid warming on centennial-scale revealed by a 2650-year stalagmite record of warm season temperature. *Geophysical Research Letters*, 30(12): 1617, doi:10.1029/2003GL017352.

Tan, M., Baker, A., Genty, D., Smith, C., Esper, J., and Cai B.G., 2006. Application of stalagmite laminae to paleoclimate reconstructions: comparison with dendrochronology/ climatology. *Quaternary Science Reviews*, 25(17): 2103–2117.

Tan Ming, 2016. Circulation background of climate patterns in the past millennium: Uncertainty analysis and re-reconstruction of ENSO-like state. *Science China* (Earth Sciences), 59(6): 1225–1241.

Teller, J.T., and Leverington, D.W., 2004. Glacier Lake Agassiz : A 5000 yr history of change and its relationship to the δ^{18}O record of Greenland. *Geological Society of Ameria Bulletin*, 116(5): 729–742.

Thomas, E.R., Wolff, E.W., Mulvaney, R., Steffensen, J.P., Johnsen, S.J., Arrowsmith, C., White, J.W.C. Vaughn, B., and Popp, T., 2007. The 8.2 ka event from Greenland ice cores. *Quaternary Science Reviews*, 26(1–2): 70–81.

Wang, Y.J., Cheng, H., Edwards, R.L., He, Y.Q., Kong, X.G., An, Z.S., Wu, J.Y., Kelly, M.J., Dykoski, C.A., and Li, X.D., 2005. The Holocene Asian monsoon: Links to solar changes and North Atlantic climate. *Science*, 308(5723): 854–857.

Wanner, H., Solomina, O., Grosjean, M., Ritz, S.P., and Jetel. M., 2011. Structure and origin of Holocene cold events. *Quaternary Science Reviews*, 30(21–22): 3109–3122.

Yin Jianjun and Tang Wei, 2016. The relationship between Local Climate/Large Scale Circualtion and δ^{18}O Recorded by Stalagmite in the Past 50 Years from Maomaotou Big Cave, Guilin. *Acta Geologica Sinica*, 90: 2035–2042 (in Chinese with English abstract).

Yang Xunlin, Zhang Pingzhong, Chen Fahu, HuH Chih-an., Li Hongchun, Cheng Hai, Johnson, K.R., Liu Jinghua and An Chunlei, 2007. Modern stalagmite oxygen isotopic composition and its implications of climatic change from a high-elevation cave in the eastern Qinghai-Tibet Plateau over the past 50 years. *Chinese Science Bulletin*, 52(9): 1238–1247.

Yang Yan, Yuan Daoxian, Cheng Hai, Zhang Meiliang, Qin Jiaming, Lin Yushi, Zhu Xiaoyan and Edwards, R.L, 2010. Precise dating of abrupt shifts in the Asian Monsoon during the last deglaciation based on stalagmite data from Yamen Cave, Guizhou Province, China. *Science China Earth Sciences*, 53(5): 633–641.

About the first author

LIU Shushang, female, was born in Yishui county, Shandong Province, China, in September 1991. She graduated from the School of resources and environmental engineering, Ludong University, Shandong, in 2016, and is currently a master degree candidate studying Physical Geography at the College of Geography Science, Nanjing Normal University, Nanjing, China. Email: Lss0817njnuv@163.com; phone: 18851837031.